Context effects on repair of 5'-overhang DSB induced by Cas12a in Arabidopsis.

Sébastien Lageix[1], Miguel Hernandez Sanchez-Rebato[1&], Maria E. Gallego[1], Jérémy Verbeke[1], Yannick Bidet[2], Sandrine Viala[2] and Charles I. White[1*]

[1] Institut de Génétique, Reproduction et Développement,
UMR CNRS 6293 - INSERM U1103 - Université Clermont Auvergne
Bât. CRBC, Faculté de Médecine. 28 place Henri Dunant.
63001 Clermont-Ferrand Cedex 1, France

[2] Laboratoire d'Oncologie Moléculaire
U1240 Imagerie Moléculaire et Stratégies Théranostiques
Université Clermont Auvergne, Centre Jean Perrin, INSERM
58 rue Montalembert, 63000 Clermont-Ferrand, France

[&] Current address: Centro de Biología Molecular Severo Ochoa,
Calle Nicolás Cabrera 1, 28049 Madrid

*Corresponding author : charles.white@cnrs.fr
ORCID: 0000-0001-8152-5797

Keywords: Recombination, DNA Repair, DSB repair, Cas12a, Arabidopsis

Abstract

Sequence-specific endonucleases have been key to the study of the mechanisms and control of DNA double-strand break (DSB) repair and recombination and the availability of CRISPR-Cas nucleases over the last decade has driven rapid progress in understanding and application of targeted recombination in many organisms, including plants. We present here an analysis of recombination at targeted chromosomal 5'overhang DSB generated by the FnCas12a endonuclease in the plant, *Arabidopsis thaliana*. The much-studied Cas9 nuclease cleaves DNA to generate blunt-ended, double-strand breaks (DSB), but relatively less is known about the repair of other types of breaks, such as those with 5'-overhanging ends.
Sequencing the repaired breaks clearly shows that the majority of repaired DSB carry small deletions and are thus repaired locally by End-Joining recombination, confirmed by Nanopore sequencing of larger amplicons. Paired DSB generate deletions at one or both cut-sites, as well as deletions and reinsertions of the deleted segment between the two cuts, visible as inversions. While differences are seen in the details, overall the deletion patterns are similar between repair at single-cut and double-cut events, notwithstanding the fact that only the former involve cohesive DNA overhangs. A strikingly different repair pattern is however

observed at breaks flanked by direct repeats. This change in sequence context results in the presence of an alternative class of repair events, corresponding to highly efficient repair by Single-strand Annealing recombination.

Introduction

DNA double-strand breaks (DSB) are highly toxic lesions, causing both local damage and separating the chromatid arm distal to the break from its centromere. This acentric chromatid can be subsequently lost, leading to loss of many genes. Alternatively either of the broken DNA ends can recombine with other sequences in the genome, to generate major structural genome rearrangements (dicentric/acentric chromosomes, deletions, translocations, inversions). A number of recombination pathways repair DSB very efficiently in living cells and the specific outcome of a given repair event is determined by the recombination mechanism involved in its repair. Thus, in somatic cells of animals and plants, chromosome breaks are predominantly repaired by DNA end-joining recombination (EJ) which, while it frequently results in mutations at the repaired break-site, avoids structural genome damage by restricting repair to sequences immediately flanking the break. Readers are referred to excellent reviews on this subject (Chang et al., 2017; Kamoen et al., 2024; Knoll et al., 2014; Scully et al., 2019; Wright et al., 2018).

The possibility to specifically induce *in vivo* breakage of a chromosomal target sequence has been key to understanding of DSB repair and its consequences and applications. Starting with the use of natural and "designer" endonucleases to cleave specific chromosomal targets, this work has been tremendously accelerated in recent years by the availability of CRISPR/Cas endonucleases. Following on from earlier work using transgenic tester loci, Zinc-finger and TALE nucleases , the application of CRISPR/Cas tools to plant models over the last decade has enabled exciting new experimental approaches, and resulted in major advances in the understanding and application of DNA repair and recombination in model and crop plants (Atia et al., 2024; Fauser et al., 2014; Gao, 2021; Jiang et al., 2013; Kamoen et al., 2024; Li et al., 2013; Nekrasov et al., 2013; Přibylová and Fischer, 2024; Schiml et al., 2016; Shan et al., 2013; Vu et al., 2017; Wolter et al., 2021; Xue and Greene, 2021).

The majority of studies DSB-induced DNA repair/recombination in plants in recent years have involved the Cas9 endonuclease and its derivatives. Sequentially cleaving the two strands of the target DNA, Cas9 generates a blunt-ended or 1-base overhang DSB (Jinek et al., 2012; Kumar et al., 2023; Longo et al., 2024; Swarts and Jinek, 2018; Weiss et al., 2024). This means that most studies of Cas9-induced breaks involve the study of blunt-ended DSB, without single-stranded (ssDNA) overhangs. The mutant Cas9-nickase protein, which cleaves only one strand, is an exception to this and has notably been used in studies of recombination at paired single-strand nicks (eg. (Bothmer et al., 2017; Fauser et al., 2014; Schiml et al., 2016, 2014)). In contrast, the Cas12a (Cpf1) endonuclease produces a staggered break, with 4-5 base 5' ssDNA overhangs at the ends (Swarts and Jinek, 2018; Zetsche et al., 2015). Furthermore, Cas12a has technical advantages which facilitate its use in studies of DSB

repair, notably that it depends upon an easily multiplexable, single guide RNA (gRNA) for targeting cleavage (Fonfara et al., 2016; Zetsche et al., 2017).

In this work we present an analysis of the patterns of DSB repair recombination following cleavage at paired genomic target sites by FnCas12a in the plant, *Arabidopsis thaliana.* The majority of repaired DSB are repaired locally by End-Joining recombination. While differences are seen in the details, overall the deletion patterns are not greatly affected by differing local sequence contexts flanking the DSB. The presence of flanking direct repeats sequences does however strongly impact the repair pattern - corresponding to highly efficient repair by Single-strand Annealing recombination.

Materials and Methods

Genomic target loci

To investigate endogenous repair profiles of CRISPR/Cas12a induced DSBs, we screened the *A. thaliana* genome sequence and selected pairs of target sites at two distinct genomic loci. The first target locus, located in the middle of the left arm of chromosome 1, corresponds to the gene *LPP2* (At1G15080). gRNAs were designed to induce two DSBs in the first intron and second exon respectively (see Figure 1a). The second target locus, Chr3_92, was identified by scanning the TAIR10 Arabidopsis genome sequence with the Tandem Repeat Finder (trf version 4.09 ; https://tandem.bu.edu/trf/trf.html) (Benson, 1999). Chr3_92 lies in the repeat-rich, pericentromeric region of Chromosome 3 and consists of two perfect 142 bp tandem direct repeats separated by 742nt. The 142 bp repeats are themselves part of two degenerate 428 bp tandem repeats. Two unique Cas12a targets were chosen in the sequences between the two repeats. The Cas12a target sites in this locus are thus flanked by tandem direct repeat DNA sequences (see Figure 5a).

T-DNA constructs and plant transformation

Recombinant CRISPR/Cas9 and sgRNA constructs (Table S1) were designed for unique genomic positions and cloned into the expression plasmids kindly provided by Dr Seiichi Toki (Endo et al., 2016). T-DNA transformation of *Arabidopsis thaliana* plants of ecotype Columbia-0 by *Agrobacterium tumefaciens* strain C58C1 was by the floral-dip method (Bechtold, N. et al., 1993; Clough and Bent, 1998).

112

113 **Plant selection**

114 In order to obtain transgenic plant lines to address specifically each of the two selected
115 targets, transformed T1 plants for each construct were grown and selected on Murashige and
116 Skoog (MS) medium (4.9 $g.l^{-1}$ Murashige and Skoog medium, 10 $g.l^{-1}$ sucrose, and 8 $g.l^{-1}$agar,
117 pH 5.7) with kanamycin (50 $\mu g.mL^{-1}$) in a growth chamber with a 16/8-hour light/dark cycle,
118 temperature 23°C and 60% relative humidity. The progeny of individuals T1 were grown for
119 10 days at 29°C on MS media and gDNA was extracted using Promega's Wizard Genomic
120 DNA Purification Kit. To assess the cutting efficiency of the transgenic lines, a PCR
121 amplifying the deletion between the two cuts sites for each target loci was performed. The T1
122 harboring the stronger activity for each construct was selected.

123

124 **Sequencing of DNA**

125 The respective target regions from 5 pooled transgenic plants each were amplified by PCR
126 (primer in Table S2) using Platinum SuperFi II DNA Polymerase (Invitrogen) and subjected to
127 NGS. Two different methods were used for NGS applications, the Illumina MiSeq and the
128 Nanopore Technology. The starting material for library preparation was 100 µL of PCR
129 products at 10 $ng{\cdot}\mu L^{-1}$. The Illumina MiSeq Nano V2 was used for paired end sequencing of
130 amplicons of a size of 400 bp. For the Nanopore Technology, library preparation was
131 conducted using the SQK-LSK110 ligation sequencing kit following the manufacturer's
132 protocol. Samples were sequenced using a minION Mk1c device using R9.4.1 (FLO-
133 MIN106D) flow cells.
134

135 **Informatics analyses.**

136 In-house Python and R scripts using publicly available tools were written to analyse the DNA
137 sequencing data produced in this study (https://github.com/chrlesw/dsbrepair.git).
138 Briefly, the scripts analyse NGS DNA sequence outputs from both Illumina paired-end
139 sequencing or Oxford Nanopore sequencing. The Nanopore sequences require no pre-
140 processing, but prior to running the analyses, the paired-end Illumina sequences are merged
141 into individual sequences using the BBMerge tool of the BBTools package (BBMap – Bushnell
142 B. – sourceforge.net/projects/bbmap/ Brian Bushnell (Bushnell et al., 2017)). These merged

143 sequence files are the input for two main Python scripts, which carries out the analysis
144 following two approaches:
145 **1) Text-recognition approach: _dsb_sortAnal.py**
146 Based on text searches and precise sequence lengths, this approach is best applied to the
147 Illumina sequences due to the lower sequencing error rate compared to Nanopore sequences.
148 The merged Illumina sequences are individually scanned for the presence/absence of the
149 Cas12a target sequence(s) using Python text-search tools. The presence of inversions is
150 identified by the presence of a reverse-complementary sequence taken from between the
151 target sites. These, combined with their lengths, are used to sort and enumerate the merged
152 sequences of different deletion classes: single site deletions, individual two-site deletions,
153 deletions spanning the two cut-sites and inversions of the sequences between the two cut-
154 sites.
155 2) **Mapping plus variant calling approach: _dsb_varAnal.py**
156 Minimap2 (Li, 2018) is used to align the Nanopore or merged, paired-end Illumina sequences
157 to the reference genome. Secondary or supplementary alignments are removed and the
158 BBMap callvariants.sh script of the BBTools package (BBMap
159 – sourceforge.net/projects/bbmap/ Brian Bushnell (Bushnell et al., 2017)) used to produce
160 lists of deletions, insertions and substitutions. Shell commands then select variants affecting
161 10 nt windows centered on the cut-sites and sort them into lists of deletions, insertions and
162 substitutions. The potential implication of DNA sequence microhomologies is determined for
163 each deletion junction and plots showing each deletion as an arc linking its start and end
164 points are generated.
165

166 ## Results

167 A FnCas12a construct expressing guide RNAs targeting two sites, LPP2_T1 and LPP2_T2,
168 respectively located in the first intron and second exon of the Lipid Phosphate Phosphatase 2
169 gene (LPP2, AT1G15080). The key characteristic of this gene as a target for this work is that it
170 is non-essential (Katagiri et al., 2005). The two target sites, T1 and T2, are 256 bp apart,
171 oriented in the same direction and both are unique in the *Arabidopsis thaliana* genome (Figure
172 1a). Stably transformed lines carrying this construct were produced by T-DNA transformation
173 and a line showing high levels of mutation at the target sites was chosen for further work. In
174 parallel a plant line carrying the same FnCas12a T-DNA construct, but lacking the gRNA
175 template was built as a -gRNA control.
176 Genomic DNA was extracted from 10-day old plantlets, a 400bp region including the target
177 sites was amplified (Figure 1a) and paired-end sequenced with an Illumina Miseq sequencer.

178 The read-pairs were merged with the BBMerge script of the BBMap package to give single
179 sequences and these were analysed by an in-house Python script (see Materials and Methods).
180
181 In principle, repair of the paired Cas12a-induced breaks can result in a number of outcomes:
182 simple religation (not detectable) or mutation of either or both T1 or T2 (Fig. 1b), deletion
183 from T1 to T2 (Fig. 1c), T1+T2 cleavage followed by re-insertion of the cut-out fragment in
184 either the original (Fig. 1d), or inverted (Fig. 1e) orientation.
185 A python script was written to quantify and sort the sequence reads into these classes. Based
186 on the sequence length plus the presence/absence of the unmodified target sequences, this
187 script gives a direct read-out of the events in each sequence. In the Cas12a+gRNA plants,
188 23644 sequences with modified T1 and/or T2 were found in the 82431 sequence reads (28.7%),
189 while 11 were found in the 52806 reads (0.02%) from the Cas12a-gRNA controls. The
190 proportions of the different classes of events found in the +gRNA sequences are shown in
191 Figure 1f. Thus, of the 28.7% of sequences which carry a deletion in T1 and/or T2, individual
192 T1 deletions (59.38%) are 2.6-fold more frequent than individual T2 deletions (23.25%),
193 presumably due to more efficient cleavage at the T1 target. 12.42% of the sequences with T1
194 and/T2 deletions have individual mutations at both T1 and T2, and 2.91% deletions
195 extending from T1-T2, with slightly lesser number (2.05%) having T1-T2 deletions associated
196 with reinsertion of the intervening sequence in inverted orientation. It is important to keep in
197 mind that the frequencies of the latter two classes (the T1-T2 events) will depend upon the
198 likelihood of a given chromatid being cleaved at both sites co-incidentally, and thus the
199 relative and absolute frequencies of cleavage at T1 and T2. The relative frequencies of these
200 paired-cut events would thus be expected to differ in different transformants, target pairs or
201 at different loci. Aligning the sorted sequence files of each class of events to the Arabidopsis
202 genome (or an in-silico T1-T2 inversion locus for the inversion sequences) confirms the
203 efficacy of this approach and gives a first view of the nature of the deletions in each class (Fig.
204 1g).
205
206 To take this analysis further, a second script was written to align the merged sequence-pairs
207 to the Arabidopsis genome and call variants with the callvariants.sh script of the BBMap
208 package (see Materials and Methods). Of 83387 sequences mapped to the LPP2 locus from the
209 Cas12a+gRNA line, deletions affecting one or both target sites represent 32.7%, insertions
210 1.0% and substitutions 4.5% (Figure 2a). As expected, very few deletions (0.02%) or insertions
211 (0.02%) were found in the 52806 sequences from the Cas12a-gRNA control, however numbers
212 of substitutions affecting the target windows were similar in the sequences from the control
213 and Cas12a+gRNA plants (3.3% versus 4.5%). Expressing these numbers as percentages of
214 detected variants (Figure 2b) gives 85.5% deletions, 2.7% insertions and 11.8% substitutions in

215 the +gRNA plantlets, and 0.58% deletions, 0.46% insertions and 98.96% substitutions in the -
216 gRNA controls. The majority of substitutions are thus not Cas12a targeted and presumably
217 arise from sequencing errors, which occur at comparable frequencies in this material .
218 The great majority of mutations induced by Cas12a at this locus are deletions and are mostly
219 short deletions. A clear, visual confirmation of this is shown in Figure 2c, which shows 1000
220 randomly-chosen deletions, each plotted as an arc joining its start- and end-points. Both the
221 clusters of small deletions at each cut-site and the larger deletions involving both cut-sites are
222 clearly visible (black arcs). It is particularly striking to note the relatively small number of
223 other deletions extending into the flanking chromosomal DNA (Figure 2c). Frequency
224 distributions of deletion lengths confirm this observation, showing clearly that, with the
225 exception of the T1-T2 deletions from 256-300bp, the great majority are less than 20bp, with
226 only rare events being longer than 60bp (Figure 2d). A similar analysis shows that practically
227 the totality of insertions are 5bp or less, with a small minority extending to 10bp (Figure 2e).
228 The FnCas12a endonuclease cleaves double-stranded DNA (dsDNA) to leave 4-5nt, 5' single-
229 strand (ssDNA) overhangs (Zetsche et al., 2015) and we expected to find a major class of 4-5nt
230 deletions corresponding to loss of the ssDNA overhangs at the cut sites, followed by
231 religation. Frequency distributions of 4 and 5nt deletion start- and end-sites confirm the
232 presence of this class of "blunting/ligation" NHEJ events (Figure 3a). This is particularly
233 clearly visible at the T1 site, where practically the totality of 4- and 5-nt deletions are at the
234 expected position. It is also seen at the T2 site, however deletions starting 2 and 3 nt upstream
235 of the expected peak are also clearly visible. Should these upstream deletion start sites result
236 from extended erosion of the upstream sequence prior to religation, this would result in
237 deletions longer than the 4-5bp and their exclusion from this analysis. We can thus
238 confidently class these events as resulting from other cleavage sites upstream of the "primary"
239 cut site.
240 Each Cas12a cut produces complementary and potentially religatable overhanging 5' ssDNA
241 ends, however this is not so for the double-cut events (deletions ≥256bp), which involve
242 joining of DNA ends from cuts in two different sequences. This distinction does not appear to
243 significantly affect the loss of sequence in the deletions, as can be seen by overlaying the
244 distributions of the 1-cut and the 2-cut events (by subtracting 256 from the lengths of the 2-cut
245 deletions) (Figure 3b). To facilitate this comparison, the frequency distributions in Figure 3b
246 are presented as fractions of total deletions. Plotting the distributions of T1 and T2 deletions
247 separately confirms that, while overall very similar, unsurprisingly there are differences in the
248 details of the patterns of deletion lengths (Figure 3c) and the choice of start and end-points
249 (Figure 3d) at the two target sites. It appears reasonable to assume that this is at the origin of
250 the minor differences between the patterns of local sequence loss in the single- and double-cut
251 EJ events (Figure 3b). Furthermore, given that the targets both lie within the LPP2 gene,

252 separated by only 256bp, these specificities are presumably due to local DNA sequence
253 context. Finally, the maximum number of nt of microhomology from 0 to 9 nt, potentially
254 involved in each deletion was calculated (see Figure S1a). Mean microhomology values for all
255 deletions starting at each coordinate were calculated across the LPP2-T1 and LPP2_T2 target
256 loci (Figure S1b and c). The number of deletions starting at each coodinate was also plotted to
257 put these values into context, confirming the absence of correlation between microhomology
258 and deletion frequency.
259
260 Due to restrictions on amplicon length for Illumina sequencing, the cut-sites analysed above
261 are 93 and 52bp from the ends of the PCR-amplified fragment used for the sequencing (Figure
262 1a). Loci with deletions extending beyond these ends would not be amplified (nor sequenced)
263 and this could clearly impact our analyses. We thus used Oxford Nanopore sequencing,
264 which doesn't suffer from these constraints on amplicon sequence length, to test whether the
265 Illumina approach had impacted our analyses and, if so, to build a clear picture of the DSB-
266 induced recombination at this locus.
267 A 2.8kb *LPP2* amplicon was chosen for Nanopore sequencing (Figure 4a). In this case, the T1
268 and T2 targets are respectively 1319bp and 1226nt from the amplicon ends. This segment was
269 amplified from 10-day old plantlets expressing the Cas12a+gRNA (targeting LPP2 as above)
270 and from plantlets expressing Cas12a+gRNA targeting another locus on chromosome 3 as
271 Cas12a-gRNA control (Chr3_92, see below). Although the Nanopore sequencing data
272 includes a significant background of small deletions and insertions, these are almost all less
273 than 6bp long (Figure 4b, c), and when excluded from the analysis, the deletion patterns from
274 the Illumina and Nanopore sequencing overlap very closely (Figure S2c).
275 Of 85439 sequences mapped to the LPP2 locus from the Cas12a+gRNA line, 48587 indels of
276 greater than 5bp affecting one or both target sites were found and of these, 98.7% were
277 deletions and 1.3% insertions (Figure S2a, S2b). As expected, very few indels >5bp (409: 379
278 deletions and 30 insertions) were found in the 87331 sequences from the Cas12a-gRNA
279 controls (Figure S2b). These numbers from the Nanopore sequencing of the 2.8kb amplicon
280 are thus comparable to those from the Illumina sequencing of the 400bp amplicon.
281 Although care needs to be taken with the totals due to the exclusion of indels of 5bp or less,
282 Nanopore sequencing of the 2.8kb amplicon does permit detection of longer indels that may
283 have been artefactually excluded from the 400bp amplicon/Illumina approach. Figure 4b
284 presents an Arc-diagram plot of 1000 random deletions of >5bp from the +gRNA Nanopore
285 sequencing and Figure 4c the frequency distribution plot of all detected deletions of >5bp.
286 Comparing Figure 4b with the equivalent plot from the Illumina sequencing (Figure 2c)
287 shows that, as expected, the longer amplicon Nanopore sequencing does permit detection of
288 deletions extending further into the sequences flanking the cut-sites than those detected with

289 the 400bp amplicon used for the Illumina sequencing. These are, however, clearly only a
290 minority of the deletions and furthermore, are restricted to the central part of the amplified
291 sequence (Figure 4c).
292 Taken together these results give a clear picture of Cas12a-induced recombination at this
293 locus in Arabidopsis plantlets, showing clearly that repair of the great majority of mutagenic
294 repair of the breaks results in short, local deletions encompassing the breakpoint. To extend
295 these conclusions and test the possible impact of different DNA sequence contexts on the
296 repair mechanisms and outcomes, we applied this approach to a second target locus, in which
297 the Cas12a target sites are flanked by tandem direct repeat DNA sequences. The chosen locus,
298 Chr3_92, lies in the repeat-rich, pericentromeric region of Chromosome 3 (Figure 5a). This
299 locus has two 142nt direct repeats separated by 742nt and two unique Cas12a targets were
300 chosen in the sequences between them. The perfect (no mismatches) 142 nt repeats are
301 themselves embedded in two mildly degenerate (18 mismatches) 428nt direct repeats (Figure
302 5a).
303 Following the same logic as for the analyses at the LPP2 locus, a 2.8Kb amplicon centered on
304 the Chr3_92 locus was amplified from 10 day-old plantlets expressing the Cas12a+gRNA
305 targeting Chr3_92_T1 and Chr3_92_T2 on chromosome 3 and a Cas12a+gRNA targeting
306 another locus as Cas12a-gRNA control (the LPP2 locus on Chromosome 1, see above). The
307 Chr3_92_T1 and Chr3_92_T2 targets, separated by 378nt, are 1361bp and 1240nt from the
308 amplicon ends respectively (Figure 5a). This 2979bp segment (Chr3:12111994-12114973) was
309 amplified by PCR and sequenced with the Oxford Nanopore Minion sequencer (as for the
310 LPP2 locus, above).
311 Of 181312 sequences mapped to the Chr3_92 locus from the Cas12a+gRNA line, 64258 indels
312 of greater than 5bp affecting one or both target sites were found and of these, 97.79% were
313 deletions and 2.21% insertions (Figure 5b, 5c). As expected, very few indels >5bp (564: 419
314 deletions and 145 insertions) were found in the 214181 sequences from the Cas12a-gRNA
315 controls (Figure 5b, 5c). These numbers from the Nanopore sequencing of the 2.8kb amplicon
316 are thus comparable to those from the Illumina sequencing of the 400bp amplicon.
317
318 Analysis of the Cas12a-induced deletions at the Chr3_92 locus shows a pattern of local
319 deletions, at and between the two cut-sites (Figure 6a), comparable to that observed at the
320 LPP2 locus (Figure 4b). However, in contrast to the LPP2 deletion pattern, a new major
321 deletion class at 742bp represents 39.37% of the 61689 deletions greater than 5bp (Figure 6a,
322 6b). 742 bp is precisely the spacing between the flanking repeat sequences and these events
323 thus presumably result from SSA recombination. The Arc-plot of the deletions confirms that
324 this is the case: a major class of deletions with start/end points distributed across the repeat
325 sequences, extend in-step from one repeat to the other (red arcs in Figure 6c). The presence of

326 these flanking direct repeat sequences thus generates a new class of recombinants
327 representing almost 40% of the total, that is not detected in their absence. The arc-plot of the
328 LPP2 deletions from Figure 3b is inset in Figure 6c for comparison.
329
330
331 The optimum temperature for activity of the FnCas12a endonuclease in plants is 29°C,
332 (Bernabé-Orts et al., 2019; Huang et al., 2021; Lee et al., 2019; Malzahn et al., 2019; Schindele
333 and Puchta, 2019) and the data presented in this article comes from analysis of plants grown
334 at this temperature. While 29°C is a temperature well within the range that Arabidopsis
335 plants will encounter in the environment and the plants grow well at this temperature, the
336 standard laboratory growth temperature for *Arabidopsis thaliana* is 23°. We thus verified that
337 the higher growth temperature doesn't impact the choice of mechanism and thus outcomes of
338 repair of Cas12a-induced DSB in the plants. Illumina sequencing of the 400bp LPP2 locus
339 amplicon from plantlets grown at 23°C and 29°C shows similar proportions of the different
340 deletion classes (Figure S3a) and the distributions of deletions (Figure S3b) and insertion
341 (Figure S3c) lengths coincide at the two temperatures. The patterns of End-Joining repair of
342 these breaks at 23° and 29° are thus equivalent. We also checked for a possible temperature-
343 specific impact on the SSA recombination pathway by making an analogous comparison
344 between results or repair of DSB targeted to the Chr3_92 locus. As for the results concerning
345 EJ recombination at the LPP2 locus (above), similar proportions of the different deletion
346 classes (Figure S4a) are observed and the distributions of deletion (Figure S4b) and insertion
347 (Figure S4c) lengths overlap at the two temperatures. The patterns of End-Joining and SSA
348 repair of 5'-overhang DSB at these two loci are thus equivalent at these two temperatures.

349

350 Discussion

351 This study concerns the repair of 5'-ssDNA overhang DSB in *Arabidopsis thaliana*, using
352 targeted *in planta* cleavage by FnCas12a (FnCpf1) (Endo et al., 2016). In addition to producing
353 5'-ssDNA overhang DSB, Cas12a has high specificity for its target and the very useful
354 capability to process precursor RNAs into crRNAs (Fonfara et al., 2016; Makarova et al., 2015;
355 Shmakov et al., 2015; Strohkendl et al., 2018; Swarts and Jinek, 2018; Zetsche et al., 2015). The
356 presence of 5' overhangs at Cas12a-induced DSB is of particular interest for study of DNA
357 break repair and recombination. Like blunt-ended and 3'-ssDNA overhang DNA breaks, 5'-
358 ssDNA overhang DSB can be repaired by simple religation. Such events are however very
359 difficult to detect and analyse, as well as being subject to further cleavage/repair.

360 Degradation of the 4-5nt 5' overhangs or filling-in of the recessed 3'-ended strands left by
361 Cas12a cleavage to generate blunt ends for EJ ligation would result in 4-5 bp deletions or
362 insertions respectively. Further resection of the 5'-ended strand would be needed to produce
363 the 3' overhangs needed for microhomology-dependent alternative end-joining (aEJ or MMEJ)
364 or homology-dependent recombination (HR) and single strand annealing (SSA).
365 As well as being less studied, notably in plants, these breaks are thus of particular interest in
366 terms of recombination. We chose to work with pairs of nearby Cas12a cuts in order to
367 characterise any specificities of repair of the (cohesive-ended) single Cas12a cuts, versus the
368 (non-cohesive-ended) twin-cuts and to check for more complex events involving re-insertion
369 of a cut-out chromosome fragment. We note also that our PCR-amplicon based analysis is
370 necessarily restricted to "local" DSB repair outcomes. While we specifically include analysis of
371 twin-break events and include long-read sequencing to take this into account, larger scale
372 rearrangements (chromosome arm loss, translocations...) are not directly analysed in the
373 work reported here. In this context, we direct readers to the recent study and discussion of
374 Cas12a-induced mutations in the ascomycete fungus *Magnaporthe oryzae* (Huang et al., 2022).
375 Finally, we note that while Cas12a enzymes are strongly impacted by protospacer/target
376 mismatches, they cut the target DNA at the PAM-distal end of the target sequence (see
377 (Strohkendl et al., 2018; Swarts and Jinek, 2018)). Thus, recognition and re-cleavage of
378 repaired targets with small sequence changes (substitutions, small indels) will potentially be
379 more frequent than would be the case with PAM-proximal cleavage by enzymes such as Cas9
380 (Swarts and Jinek, 2018). While this effet could be expected to lead to longer deletions, our
381 results however show a marked predominance of very short deletions, suggesting that the
382 impact of this in our plants is less than might have been expected, perhaps due to the very
383 efficient cutting.
384
385 Five principle conclusions emerge from the work presented here:
386 1) The great majority of mutations left by the repair of these 5'-overhang DSB are deletions,
387 with a clear peak of deletion lengths at 4bp. The frequencies then fall off rapidly with
388 increasing deletion length. Strikingly, repair resulting in insertions (also very short) is > 30-
389 fold less frequent than that producing deletions. Examination of the patterns of deletion
390 lengths shows them to be very similar at the different cut-sites, with however some
391 differences seen in the details (see below). Plotting mean microhomology length against
392 deletion start point across the target sites shows no clear evidence for a relation between the
393 probability of a given base pair serving as the start-point of a deletion and the mean number
394 of nt of microhomology potentially involved in the deletions starting at that position in the
395 sequence. While the existence of such microhomologies in the sequence in no way proves
396 that they were actually involved in the recombination event under study, this result does

397 indicate that the use of longer microhomolgies is not a primary determinant in the choice of
398 the start and end-points of these very short deletions resulting from repair of 5'-overhang DSB
399 in Arabidopsis.
400
401 2) The proximity of the FnCas12a cut-sites to the ends of the 400bp LPP2 amplicon used for
402 Illumina sequencing could clearly impact the patterns of deletions found in this work,
403 excluding repair events involving longer deletions. We thus amplified a 2.8 Kb fragment
404 covering the same locus, for sequencing with the Oxford Nanopore Minion sequencer. The
405 two FnCas12a cut-sites are 1319 and 1226 bp from the ends of this 2.8 Kb amplicon,
406 considerably more distant than the 93 and 51bp in the 400 bp amplicon. Strikingly, while the
407 results of sequencing the longer amplicon did permit identification of longer deletions, these
408 were increasingly rare with increasing length and the overall pattern of repair wasn't changed
409 relative to that from the 400 bp amplicon sequencing.
410
411 3) The use of nearby pairs of Cas12a targets results in a spectrum of modifications at the
412 repaired cuts: individual, local deletions at one or both targets, and deletion and inversions of
413 the DNA sequences between the two targets (Figure 1). While the relative proportions of
414 "one-cut" versus "two-cut" events will be dependent upon the relative and absolute cutting
415 efficiencies at the two sites, examination of the "excision" events involving coincident cutting
416 of both target sites does yield some interesting conclusions. These include the 2.91% of
417 sequences with deletions spanning the two cut sites (T1-T2 deletions) and the events
418 involving reinsertion of the excised T1-T2 fragment. Depending on the orientation of the
419 reinsertion of the excised fragment, the "excision-reinsertion" events would include both the
420 2.05% of sequences with T1-T2 inversions and an equivalent number classed within the
421 12.42% of sequences with local deletions at both T1 and T2. Thus the excision-reinsertion class
422 would represent ~4% of sequences. That this value is comparable in magnitude to the number
423 of T1 to T2 deletions (excision without reinsertion (~3%) suggests that loss or reinsertion of
424 the excised fragmant in two-site cleavage events are equally likely.
425
426 4) The use of paired target sites permitted analysis of patterns of deletions at junctions
427 resulting from joining DNA ends with complementary 5'-overhangs (1-cut deletions) and at
428 those involving non-complementary 5'-overhangs (two-cut deletions). The two cut-sites are
429 separated by 256 bp and subtracting this from the lengths of the T1-T2 deletions permits
430 overlaying the pattern of the T1-T2 deletions with the 1-cut events. While some differences are
431 made clearly visible by this approach, the predominance of 4 bp deletions, followed by a
432 rapid fall-off with increasing deletion-length is strikingly similar. Thus, the presence/absence
433 of cohesive 5' overhangs does not affect the deletion pattern.

5) The pattern of EJ repair of the 5'-overhang DSB thus results overwhelmingly in the production of very short deletions, with the precise details of the deletion end-points being impacted by local sequence context. This is the case for the two target sites in the chromosome-arm, expressed LPP2 gene and the two targets in the pericentromeric, heterochromatic Chr3_92 locus. The Chr3_92 cut-sites are flanked by tandem direct repeat sequences and this leads to the presence of a new class of deletion events resulting from Single-Strand Annealing (SSA) recombination. It is particularly striking that these SSA events are a major repair class, greatly outnumbering the 2-cut deletions and approaching in frequency the EJ repair events (39% versus 61% of deletions respectively). It is possible that these events result from microhomology-mediate end-joining of a sequence close to the cut site with a target in the flanking repeat. That this is not so is seen clearly in the fact that, rather than being concentrated close to the cut-sites, the start and end-points of the SSA deletions are distributed throughout the (degenerate) repeat sequences. The presence of these flanking direct repeats thus leads to a striking change in the pattern of repair, channeling almost 40% of events into the SSA pathway.

Acknowledgements

We thank Olivier Mathieu, Yoan Renaud and the members of the recombination group for their help and suggestions.
This work was supported by the Agence National de Recherche (ANR-16-CE91-0010-01 RecInChromatin), the European Marie Sklodowska Curie Actions (EU H2020-MSCA-ITN-2017-765212), the Centre National de Recherche Scientifique (CNRS), the Institut National de la Santé et de la Recherche Médicale (Inserm) and the Université Clermont Auvergne.

Data Statement

The sequence files are available under BioProject accession number PRJNA1113952 at https://www.ncbi.nlm.nih.gov/sra/PRJNA1113952 (Biosample Accessions: SAMN41471278, SAMN41471279, SAMN41471280, SAMN41471281, SAMN41471282, SAMN41471283, SAMN41488828, SAMN41488829, SAMN41488830).
The Python and R scripts using publicly available tools written to analyse the DNA sequencing data produced in this study can be downloaded from:
https://github.com/chrlesw/dsbrepair.git

467

468 ## Supporting Information

469 **Supporting Figures and Tables:**

470 **Figure S1. Potential implication of microhomologies in deletion formation.**

471 **Figure S2. Cas12a-induced Indel patterns are confirmed by 2.8 Kb amplicon Nanopore**

472 **Figure S3. Cas12a-induced Indel patterns at the LPP2 locus from plants grown at 23°C and**
473 **29°C.**

474 **Figure S4. Cas12a-induced Indel patterns at the Chr3_92 locus from plants grown at 23°C and**
475 **29°C.**

476 **Table S1. DNA sequences used for sgRNA constructs.**

477 **Table S2. List of primers used in this study.**

478

479 ## Author Contributions

480 Designed Research and Analysis: SL, MG, YB, MH, CIW; Carried out experiments: SL, MG,
481 MH, SV, JV, CIW; Resources: MG, YB, CIW;
482 Writing, with contributions from all of the authors: SL, MG, CIW.

483
484 ## Conflict of Interest
485 We declare no financial or other conflicts of interest in this work.
486
487

488 ## Figure Legends

489 **Figure 1. Patterns of repair of paired, 5'-overhang DNA breaks at the LPP2 locus.**

490 (a) A schematic showing the two Cas12a target sites of the target LPP2 locus and the 400 bp
491 amplicon used for paired-end sequencing. The sequence, including the (TTT) PAM and the
492 23nt protospacer, of the targets is shown along with staggered red lines indicating the
493 expected cleavage of the target DNA strands. Cleavage of one or both targets is expected to
494 result in mutation of one or both targets (b). Coincident cleavage at both sites can result in
495 deletion of the DNA fragment between the two targets (c ; T1-T2 deletion), possibly

496 accompanied by its reinsertion in either the original (d ; not distinguishable from T1 and T2
497 mutated class (b)), or inverted (e ; T1-T2 inversion) orientation. (f) Sorting the paired-end
498 sequences spanning the target locus confirmed the existence and relative proportions of these
499 different classes of event induced in the genome of plants expressing Cas12a. (g) The validity
500 of the sorting is confimed by mapping the sequences of the different repair classes to the
501 Arabidopsis genome, or to an artifical *in silico* inversion locus for the T1-T2_inversion class
502 (bottom).
503
504 **Figure 2. Deletions predominate in the repair of 5'-overhang DNA breaks at the LPP2 locus.**

505 (a, b) Analysis of variants affecting 10 bp windows centered on the cut-sites confirms the
506 predominance of deletions in the repair products of Cas12a-induced breaks at the LPP2 locus.
507 DNA from the -gRNA control plants contains almost exclusively base-substitutions,
508 presumably resulting from sequencing errors. (c) Plotting 1000 randomly-chosen deletions as
509 arcs (arcs from start to end of deletion) across the target locus (X-axis, horizontal orange bar),
510 shows that the deletions are almost exclusively focussed locally at the cut-sites or span
511 between them. This is confirmed by plotting the distributions of the numbers of deletions (d)
512 and insertions (e) by their lengths (blue curves are +gRNA and red are -gRNA controls).
513 Vertical orange lines in (c) mark the target-sites.
514
515 **Figure 3. Patterns of deletions at the LPP2_T1 and LPP2_T2 targets.**

516 (a) Frequency distributions of start-sites (blue) and end-sites (red) of 4 and 5nt deletion
517 affecting the 10 bp windows centered on the cut-sites. The red bars have been offset slightly to
518 the right for clarity. The target locus sequence with the cut-sites marked by staggered red
519 lines, is shown below the graph. Vertical dotted lines show the centers of the cut-sites to
520 facilitate lecture of the graphs. The majority of these deletions begin at the base pair
521 immediately upstream of the 5' ssDNA overhang produced by Cas12a cleavage of the
522 LPP2_T1 target, and the end points are found 4 and 5 bases downstream. The LPP2_T2 target
523 has 3 preferred start-points for 4 and 5nt deletions, including deletions starting 2 and 3 nt
524 upstream of the expected cut. (b) Frequency distributions of lengths of single-cut and double-
525 cut (transposed 256nt leftwards) confirm that the deletion patterns of the majority, small local
526 deletions aren't affected by the presence of cohesive (1-cut) versus non-cohesive (2-cut) 5'
527 ssDNA overhanging ends. Taken individually, frequency distributions of deletion lengths (c)
528 and deletion start- and end-points (d ; same presentation as in (a)) at the two cut-sites are
529 dominated by short local events, notwithstanding the presence of differences in the details of
530 the distributions at the two sites.
531

532 **Figure 4. Nanopore sequencing confirms patterns of Cas12a-induced deletions at the LPP2**
533 **targets.**

534 (a) Schematic showing the two Cas12a target sites of the target LPP2 locus and the 2.8 Kb
535 amplicon used for Nanopore sequencing. (b) Plot showing arcs linking each deletion start-
536 and end-point across the target locus (X-axis, horizontal orange bar). Vertical orange lines
537 mark the target-sites. The arcs are all of the same grey colour, the darker lines reflect
538 overlaying of multiple arcs. (c) Distributions of numbers of deletions by their lengths in
539 Cas12a+gRNA plants (blue curve) and Cas12a-gRNA controls (red curve). Deletions of less
540 than 5 bp were excluded due to the high background of small indel errors in Nanopore
541 sequences.
542
543 **Figure 5. Patterns of Cas12a-induced deletions at the Chr3_92 target locus.**

544 (a) Schematic showing the two Cas12a target sites flanked by direct-repeat sequences of the
545 target Chr3_92 locus and the 2.979 Kb amplicon used for Nanopore sequencing. The target
546 sequences, including the (TTT) PAM and the 23nt protospacer, are shown along with
547 staggered red lines indicating the expected cleavage of the target DNA strands. (b) Numbers
548 of sequences and the deletions and insertions expressed as fractions of mapped to the
549 Chr3_92 locus from Cas12a+gRNA (blue) and Cas12a-gRNA plants (red). Indels of less than 5
550 bp were excluded due to the high background of small indel errors in Nanopore sequences.
551 (c) As seen at the LPP2 locus, the majority of Cas12a-induced indels are deletions (b, c).
552
553 **Figure 6. The presence of flanking direct-repeats generates a major new class of Single-Strand**
554 **Annealing deletions.**

555 (a) Distributions of numbers of deletions by their lengths in Cas12a+gRNA plants (blue curve)
556 and Cas12a-gRNA controls (red curve). Deletions of less than 5 bp were excluded due to the
557 high background of small indel errors in Nanopore sequences. A major (39.4%), novel class of
558 742 bp deletions is created by the presence of the direct repeats flanking the Cas12a target
559 sites. (c) Deletion start-end arc-plots confirm that these 742 bp deletions (red curves) result
560 from in-step recombination between the flanking direct-repeats, as expected from SSA
561 recombination. This is strikingly different from the patters observed at the LPP2 locus in the
562 absence of the flanking repeats (inset in (c), repeated from Figure 4).
563

564 ## Supporting Figure Legends

565 **Supporting Figure S1. Potential implication of microhomologies in deletion formation.**

566 (a) The maximum number of nt of microhomology, from 0 to 9 nt, by comparing the
567 sequences of the upstream DSB-end with the downstream end of the deletion, and the
568 downstream DSB-end with the upstream end of the deletion (black bars connected by dotted
569 lines). The lengths of such microhomologies, potentially involved in the deletion, were
570 determined for each deletion and the mean microhomology values calculated for each
571 deletion start-point across the target sequence. These are plotted as vertical blue bars for the
572 sequences upstream of the LPP2_T1 (b) and LPP2_T2 (c) targets. The number of deletions
573 starting at each start-point are overlaid (red curve) and the cut-site (vertical dotted lines) are
574 included for reference.
575

576 **Supporting Figure S2. Cas12a-induced Indel patterns are confirmed by 2.8 Kb amplicon**
577 **Nanopore sequencing.**

578 (a) Numbers of sequences and the deletions and insertions expressed as fractions of mapped
579 to the LPP2 locus from Cas12a+gRNA (blue) and Cas12a-gRNA plants (red). Indels of less
580 than 5 bp were excluded due to the high background of small indel errors in Nanopore
581 sequences. As seen from the Illumina sequencing of the 400 bp amplicon (Fig. 2), the majority
582 of Cas12a-induced indels are deletions (a, b). Deletion-length frequency distributions from the
583 400 bp paired-end Illumina (blue curve) and 2.8 Kb Nanopore (red curve) sequencing data (c).
584

585 **Supporting Figure S3. Cas12a-induced Indel patterns at the LPP2 locus from plants grown at**
586 **23°C and 29°C.**

587 Illumina sequencing of the 400bp LPP2 locus amplicon from plantlets grown at 23°C and 29°C
588 shows similar proportions of the different deletion classes (a). This is also seen in the
589 distributions of deletion-lengths (b) and insertion-lengths (c) from plantlets grown at 29° (blue
590 curves) and 23° (red curves).
591

592 **Supporting Figure S4. Cas12a-induced Indel patterns at the Chr3_92 locus from plants grown**
593 **at 23°C and 29°C.**

594 Nanopore sequencing of the 2.8 Kb Chr3_92 locus amplicon from plantlets grown at 23°C and
595 29°C shows similar proportions of the different deletion classes (a). This is also seen in the
596 distributions of deletion-lengths (b) and insertion-lengths (c) from plantlets grown at 29° (blue
597 curves) and 23° (red curves).

598

599 **Table S1. DNA sequences used for sgRNA constructs.**

600

601 **Table S2. List of primers used in this study.**

602

603 Bibliography

604

605 Atia, M., Jiang, W., Sedeek, K., Butt, H., Mahfouz, M., 2024. Crop bioengineering via gene editing:
606 reshaping the future of agriculture. Plant Cell Rep 43, 98. https://doi.org/10.1007/s00299-024-03183-1
607 Bechtold, N., Ellis, J., Pelletier, G., 1993. In planta Agrobacterium-mediated gene transfer by
608 infiltration of adult Arabidopsis thaliana plants. C. R. Acad. Sci. Paris, Life Sci. 1194–1199.
609 Benson, G., 1999. Tandem repeats finder: a program to analyze DNA sequences. Nucleic Acids
610 Research 27, 573–580. https://doi.org/10.1093/nar/27.2.573
611 Bernabé-Orts, J.M., Casas-Rodrigo, I., Minguet, E.G., Landolfi, V., Garcia-Carpintero, V., Gianoglio,
612 S., Vázquez-Vilar, M., Granell, A., Orzaez, D., 2019. Assessment of Cas12a-mediated gene editing
613 efficiency in plants. Plant Biotechnol J 17, 1971–1984. https://doi.org/10.1111/pbi.13113
614 Bothmer, A., Phadke, T., Barrera, L.A., Margulies, C.M., Lee, C.S., Buquicchio, F., Moss, S.,
615 Abdulkerim, H.S., Selleck, W., Jayaram, H., Myer, V.E., Cotta-Ramusino, C., 2017. Characterization
616 of the interplay between DNA repair and CRISPR/Cas9-induced DNA lesions at an endogenous locus.
617 Nat Commun 8, 13905. https://doi.org/10.1038/ncomms13905
618 Bushnell, B., Rood, J., Singer, E., 2017. BBMerge – Accurate paired shotgun read merging via overlap.
619 PLOS ONE 12, e0185056. https://doi.org/10.1371/journal.pone.0185056
620 Chang, H.H.Y., Pannunzio, N.R., Adachi, N., Lieber, M.R., 2017. Non-homologous DNA end joining
621 and alternative pathways to double-strand break repair. Nat Rev Mol Cell Biol 18, 495–506.
622 https://doi.org/10.1038/nrm.2017.48
623 Clough, S.J., Bent, A.F., 1998. Floral dip: a simplified method for Agrobacterium -mediated
624 transformation of Arabidopsis thaliana. The Plant Journal 16, 735–743. https://doi.org/10.1046/j.1365-
625 313x.1998.00343.x
626 Endo, A., Masafumi, M., Kaya, H., Toki, S., 2016. Efficient targeted mutagenesis of rice and tobacco
627 genomes using Cpf1 from Francisella novicida. Sci Rep 6, 38169. https://doi.org/10.1038/srep38169
628 Fauser, F., Schiml, S., Puchta, H., 2014. Both CRISPR/Cas-based nucleases and nickases can be used
629 efficiently for genome engineering in Arabidopsis thaliana. The Plant journal : for cell and molecular
630 biology 79, 348–359. https://doi.org/10.1111/tpj.12554
631 Fonfara, I., Richter, H., Bratovič, M., Le Rhun, A., Charpentier, E., 2016. The CRISPR-associated
632 DNA-cleaving enzyme Cpf1 also processes precursor CRISPR RNA. Nature 532, 517–521.
633 https://doi.org/10.1038/nature17945
634 Gao, C., 2021. Genome engineering for crop improvement and future agriculture. Cell 184, 1621–1635.
635 https://doi.org/10.1016/j.cell.2021.01.005
636 Huang, J., Rowe, D., Subedi, P., Zhang, W., Suelter, T., Valent, B., Cook, D.E., 2022. CRISPR-Cas12a
637 induced DNA double-strand breaks are repaired by multiple pathways with different mutation profiles
638 in Magnaporthe oryzae. Nat Commun 13, 7168. https://doi.org/10.1038/s41467-022-34736-1
639 Huang, T., Armstrong, B., Schindele, P., Puchta, H., 2021. Efficient gene targeting in Nicotiana
640 tabacum using CRISPR/SaCas9 and temperature tolerant LbCas12a. Plant Biotechnol J 19, 1314–1324.
641 https://doi.org/10.1111/pbi.13546
642 Jiang, W., Zhou, H., Bi, H., Fromm, M., Yang, B., Weeks, D.P., 2013. Demonstration of

CRISPR/Cas9/sgRNA-mediated targeted gene modification in Arabidopsis, tobacco, sorghum and rice. Nucleic Acids Research 41, e188. https://doi.org/10.1093/nar/gkt780

Jinek, M.M., Chylinski, K.K., Fonfara, I.I., Hauer, M.M., Doudna, J.A.J., Charpentier, E.E., 2012. A programmable dual-RNA-guided DNA endonuclease in adaptive bacterial immunity. Science (New York, NY) 337, 816–821. https://doi.org/10.1126/science.1225829

Kamoen, L., Kralemann, L.E.M., Van Schendel, R., Van Tol, N., Hooykaas, P.J.J., De Pater, S., Tijsterman, M., 2024. Genetic dissection of mutagenic repair and T-DNA capture at CRISPR-induced DNA breaks in *Arabidopsis thaliana*. PNAS Nexus pgae094. https://doi.org/10.1093/pnasnexus/pgae094

Katagiri, T., Ishiyama, K., Kato, T., Tabata, S., Kobayashi, M., Shinozaki, K., 2005. An important role of phosphatidic acid in ABA signaling during germination in *Arabidopsis thaliana*. The Plant Journal 43, 107–117. https://doi.org/10.1111/j.1365-313X.2005.02431.x

Knoll, A., Fauser, F., Puchta, H., 2014. DNA recombination in somatic plant cells: mechanisms and evolutionary consequences. Chromosome research. https://doi.org/10.1007/s10577-014-9415-y

Kumar, J., Char, S.N., Weiss, T., Liu, H., Liu, B., Yang, B., Zhang, F., 2023. Efficient protein tagging and cis-regulatory element engineering via precise and directional oligonucleotide-based targeted insertion in plants. The Plant Cell 35, 2722–2735. https://doi.org/10.1093/plcell/koad139

Lee, K., Zhang, Y., Kleinstiver, B.P., Guo, J.A., Aryee, M.J., Miller, J., Malzahn, A., Zarecor, S., Lawrence-Dill, C.J., Joung, J.K., Qi, Y., Wang, K., 2019. Activities and specificities of CRISPR/Cas9 and Cas12a nucleases for targeted mutagenesis in maize. Plant Biotechnol J 17, 362–372. https://doi.org/10.1111/pbi.12982

Li, H., 2018. Minimap2: pairwise alignment for nucleotide sequences. Bioinformatics 34, 3094–3100. https://doi.org/10.1093/bioinformatics/bty191

Li, J.-F., Norville, J.E., Aach, J., McCormack, M., Zhang, D., Bush, J., Church, G.M., Sheen, J., 2013. Multiplex and homologous recombination–mediated genome editing in Arabidopsis and Nicotiana benthamiana using guide RNA and Cas9. Nature Biotechnology 31, 688–691. https://doi.org/10.1038/nbt.2654

Longo, G.M.C., Sayols, S., Kotini, A.G., Heinen, S., Möckel, M.M., Beli, P., Roukos, V., 2024. Linking CRISPR–Cas9 double-strand break profiles to gene editing precision with BreakTag. Nat Biotechnol 1–15. https://doi.org/10.1038/s41587-024-02238-8

Makarova, K.S., Wolf, Y.I., Alkhnbashi, O.S., Costa, F., Shah, S.A., Saunders, S.J., Barrangou, R., Brouns, S.J.J., Charpentier, E., Haft, D.H., Horvath, P., Moineau, S., Mojica, F.J.M., M, T.R., P, T.M., White, M.F., Yakunin, A.F., Garrett, R.A., Oost, J. van der, Backofen, R., Koonin, E.V., 2015. An updated evolutionary classification of CRISPR-Cas systems. Nature Reviews Microbiology 13, 722–736. https://doi.org/10.1038/nrmicro3569

Malzahn, A.A., Tang, X., Lee, K., Ren, Q., Sretenovic, S., Zhang, Yingxiao, Chen, H., Kang, M., Bao, Y., Zheng, X., Deng, K., Zhang, T., Salcedo, V., Wang, K., Zhang, Yong, Qi, Y., 2019. Application of CRISPR-Cas12a temperature sensitivity for improved genome editing in rice, maize, and Arabidopsis. - PubMed - NCBI. BMC Biology 17, 9. https://doi.org/10.1186/s12915-019-0629-5

Nekrasov, V., Staskawicz, B., Weigel, D., Jones, J.D.G., Kamoun, S., 2013. Targeted mutagenesis in the model plant Nicotiana benthamiana using Cas9 RNA-guided endonuclease. Nature Biotechnology 31, 691–693. https://doi.org/10.1038/nbt.2655

Přibylová, A., Fischer, L., 2024. How to use CRISPR/Cas9 in plants: from target site selection to DNA repair. Journal of Experimental Botany erae147. https://doi.org/10.1093/jxb/erae147

Schiml, S., Fauser, F., Puchta, H., 2016. Repair of adjacent single-strand breaks is often accompanied by the formation of tandem sequence duplications in plant genomes. Proceedings of the National Academy of Sciences of the United States of America 113, 7266–7271. https://doi.org/10.1073/pnas.1603823113

Schiml, S., Fauser, F., Puchta, H., 2014. The CRISPR/Cas system can be used as nuclease for in planta gene targeting and as paired nickases for directed mutagenesis in Arabidopsis resulting in heritable progeny. The Plant journal : for cell and molecular biology 80, 1139–1150. https://doi.org/10.1111/tpj.12704

695 Schindele, P., Puchta, H., 2019. Engineering CRISPR/ LbCas12a for highly efficient, temperature-
696 tolerant plant gene editing. Plant Biotechnology Journal 17, 1971–3. https://doi.org/10.1111/pbi.13275
697 Scully, R., Panday, A., Elango, R., Willis, N.A., 2019. DNA double-strand break repair-pathway choice
698 in somatic mammalian cells. Nat Rev Mol Cell Biol 20, 698–714. https://doi.org/10.1038/s41580-019-
699 0152-0
700 Shan, Q., Wang, Y., Li, J., Zhang, Y., Chen, K., Liang, Z., Zhang, K., Liu, J., Xi, J.J., Qiu, J.-L., Gao,
701 C., 2013. Targeted genome modification of crop plants using a CRISPR-Cas system. Nature
702 Biotechnology 31, 686–688. https://doi.org/10.1038/nbt.2650
703 Shmakov, S., Abudayyeh, O.O., Makarova, K.S., Wolf, Y.I., Gootenberg, J.S., Semenova, E.,
704 Minakhin, L., Joung, J., Konermann, S., Severinov, K., Zhang, F., Koonin, E.V., 2015. Discovery and
705 Functional Characterization of Diverse Class 2 CRISPR-Cas Systems. Molecular Cell 60, 385–397.
706 https://doi.org/10.1016/j.molcel.2015.10.008
707 Strohkendl, I., Saifuddin, F.A., Rybarski, J.R., Finkelstein, I.J., Russell, R., 2018. Kinetic Basis for
708 DNA Target Specificity of CRISPR-Cas12a. Molecular Cell 71, 816-824.e3.
709 https://doi.org/10.1016/j.molcel.2018.06.043
710 Swarts, D.C., Jinek, M., 2018. Cas9 versus Cas12a/Cpf1: Structure–function comparisons and
711 implications for genome editing. WIREs RNA 9, e1481. https://doi.org/10.1002/wrna.1481
712 Vu, G.T.H., Cao, H.X., Fauser, F., Reiss, B., Puchta, H., Schubert, I., 2017. Endogenous sequence
713 patterns predispose the repair modes of CRISPR/Cas9-induced DNA double-stranded breaks in
714 Arabidopsis thaliana. Plant J 92, 57–67. https://doi.org/10.1111/tpj.13634
715 Weiss, T., Kumar, J., Chen, C., Guo, S., Schlegel, O., Lutterman, J., Ling, K., Zhang, F., 2024. Dual
716 activities of an X-family DNA polymerase regulate CRISPR-induced insertional mutagenesis across
717 species. Nat Commun 15, 6293. https://doi.org/10.1038/s41467-024-50676-4
718 Wolter, F., Schindele, P., Beying, N., Scheben, A., Puchta, H., 2021. Different DNA repair pathways
719 are involved in single-strand break-induced genomic changes in plants. The Plant Cell 33, 3454–3469.
720 https://doi.org/10.1093/plcell/koab204
721 Wright, W.D., Shah, S.S., Heyer, W.-D., 2018. Homologous recombination and the repair of DNA
722 double-strand breaks. J Biol Chem 293, 10524–10535. https://doi.org/10.1074/jbc.TM118.000372
723 Xue, C., Greene, E.C., 2021. DNA Repair Pathway Choices in CRISPR-Cas9-Mediated Genome
724 Editing. Trends in Genetics 37, 639–656. https://doi.org/10.1016/j.tig.2021.02.008
725 Zetsche, B., Gootenberg, J.S., Abudayyeh, O.O., Slaymaker, I.M., Makarova, K.S., Essletzbichler, P.,
726 Volz, S.E., Joung, J., Oost, J. van der, Regev, A., Koonin, E.V., Zhang, F., 2015. Cpf1 is a single RNA-
727 guided endonuclease of a class 2 CRISPR-Cas system. Cell 163, 759–771.
728 https://doi.org/10.1016/j.cell.2015.09.038
729 Zetsche, B., Heidenreich, M., Mohanraju, P., Fedorova, I., Kneppers, J., DeGennaro, E.M., Winblad,
730 N., Choudhury, S.R., Abudayyeh, O.O., Gootenberg, J.S., Wu, W.Y., Scott, D.A., Severinov, K., Oost,
731 J. van der, Zhang, F., 2017. Multiplex gene editing by CRISPR-Cpf1 using a single crRNA array.
732 Nature Biotechnology 35, 31–34. https://doi.org/10.1038/nbt.3737
733

Figure 1

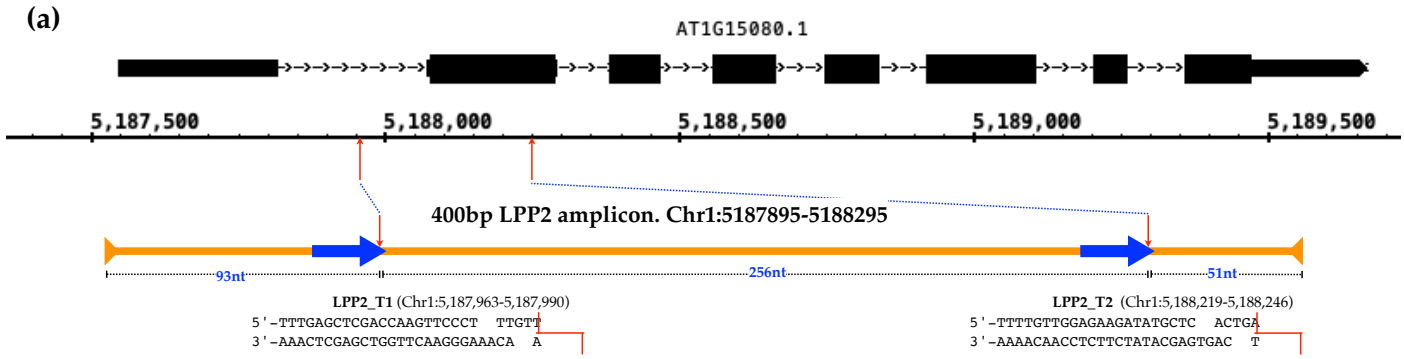
(a)
AT1G15080.1
5,187,500
5,188,000
5,188,500
5,189,000
5,189,500
400bp LPP2 amplicon. Chr1:5187895-5188295
93nt
256nt
51nt
LPP2_T1 (Chr1:5,187,963-5,187,990)
5'-TTTGAGCTCGACCAAGTTCCCT TTGTT
3'-AAACTCGAGCTGGTTCAAGGGAAACA A
LPP2_T2 (Chr1:5,188,219-5,188,246)
5'-TTTTGTTGGAGAAGATATGCTC ACTGA
3'-AAAACAACCTCTTCTATACGAGTGAC T

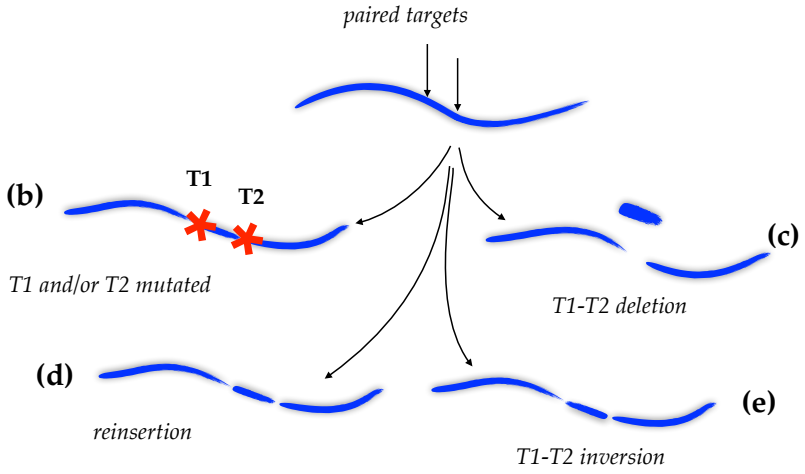
paired targets
(b)
T1
T2
T1 and/or T2 mutated
(c)
T1-T2 deletion
(d)
reinsertion
(e)
T1-T2 inversion

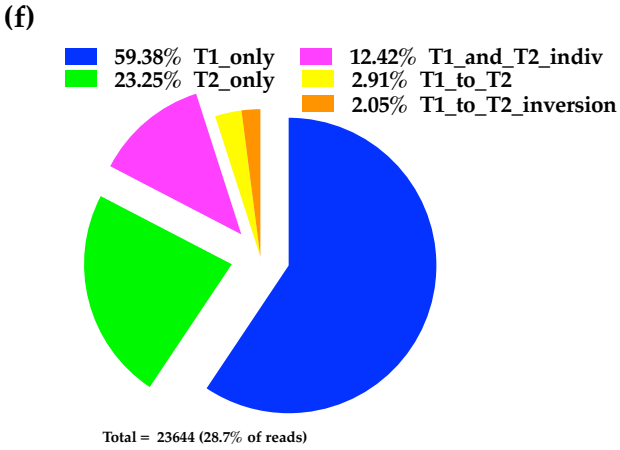
(f)
59.38% T1_only
23.25% T2_only
12.42% T1_and_T2_indiv
2.91% T1_to_T2
2.05% T1_to_T2_inversion
Total = 23644 (28.7% of reads)

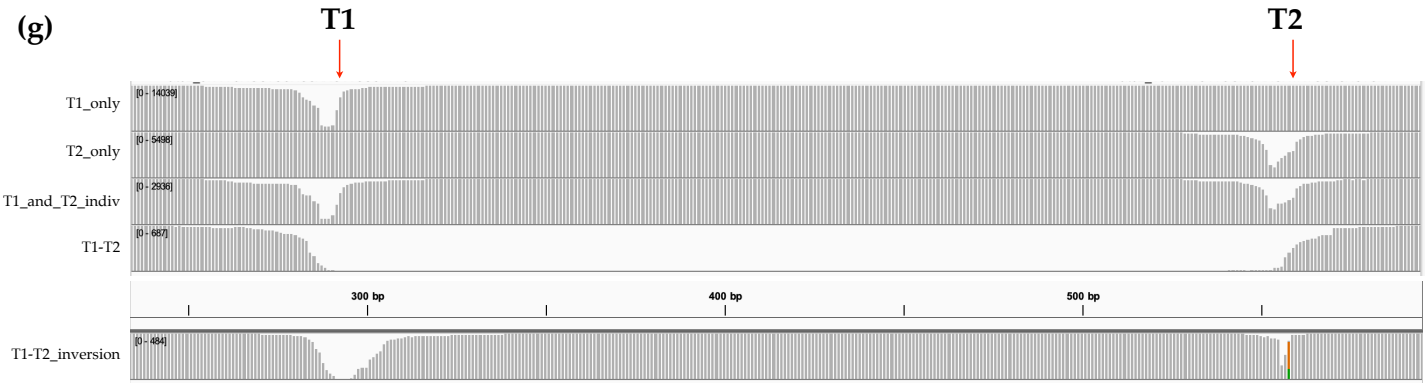
(g)
T1
T2
T1_only
T2_only
T1_and_T2_indiv
T1-T2
300 bp
400 bp
500 bp
T1-T2_inversion

Figure 2

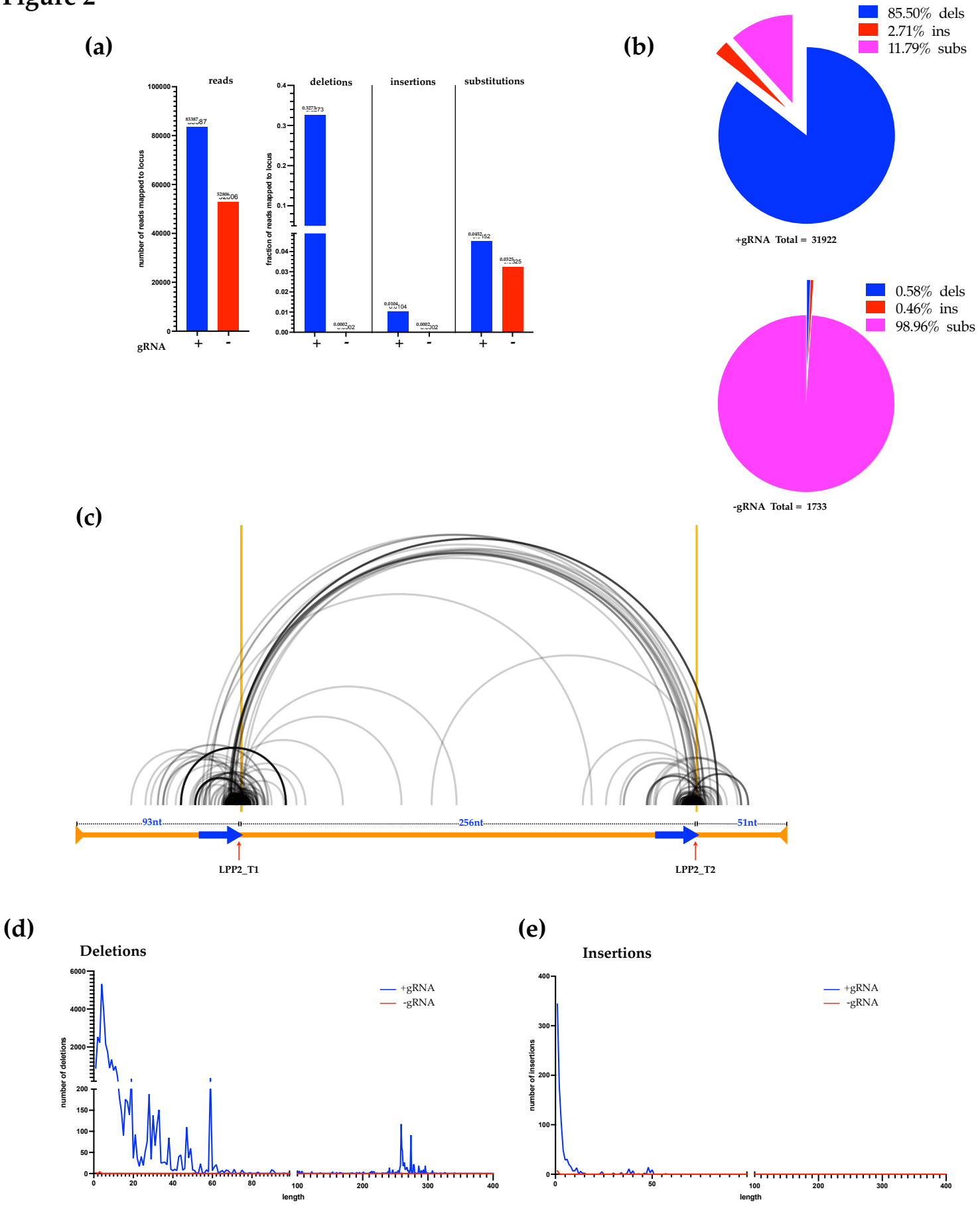
(a)
reads
deletions
insertions
substitutions
number of reads mapped to locus
fraction of reads mapped to locus
gRNA
+
-
(b)
85.50% dels
2.71% ins
11.79% subs
+gRNA Total = 31922
0.58% dels
0.46% ins
98.96% subs
-gRNA Total = 1733
(c)
93nt
256nt
51nt
LPP2_T1
LPP2_T2
(d)
Deletions
+gRNA
-gRNA
number of deletions
length
(e)
Insertions
+gRNA
-gRNA
number of insertions
length

Figure 3

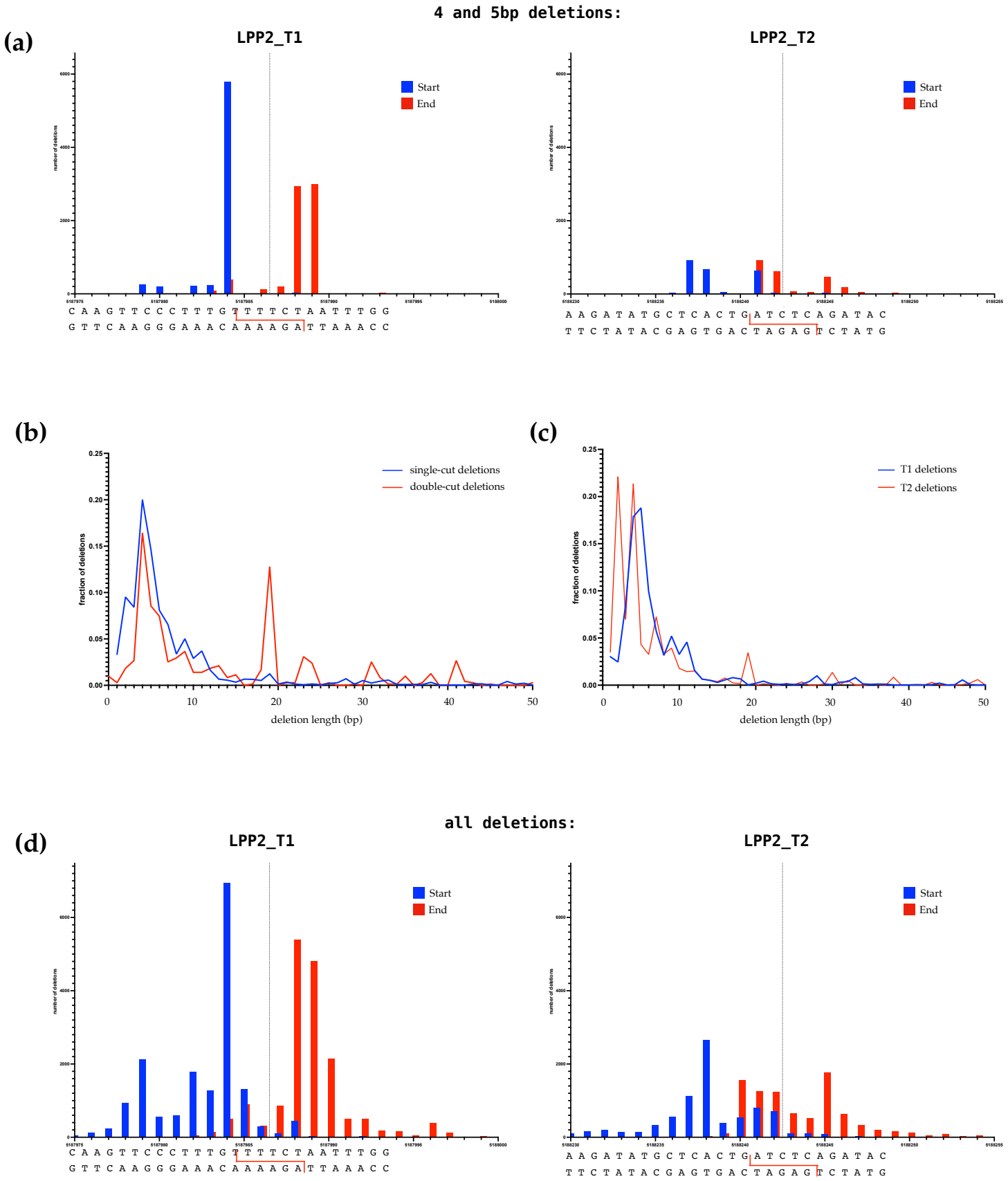
4 and 5bp deletions:
(a)
LPP2_T1
LPP2_T2
Start
End
number of deletions
C A A G T T C C C T T T G T T T T C T A A T T T G G
G T T C A A G G G A A A C A A A A G A T T A A A C C
A A G A T A T G C T C A C T G A T C T C A G A T A C
T T C T A T A C G A G T G A C T A G A G T C T A T G
(b)
single-cut deletions
double-cut deletions
fraction of deletions
deletion length (bp)
(c)
T1 deletions
T2 deletions
fraction of deletions
deletion length (bp)
all deletions:
(d)
LPP2_T1
LPP2_T2
Start
End
number of deletions
C A A G T T C C C T T T G T T T T C T A A T T T G G
G T T C A A G G G A A A C A A A A G A T T A A A C C
A A G A T A T G C T C A C T G A T C T C A G A T A C
T T C T A T A C G A G T G A C T A G A G T C T A T G

Figure 4

(a)

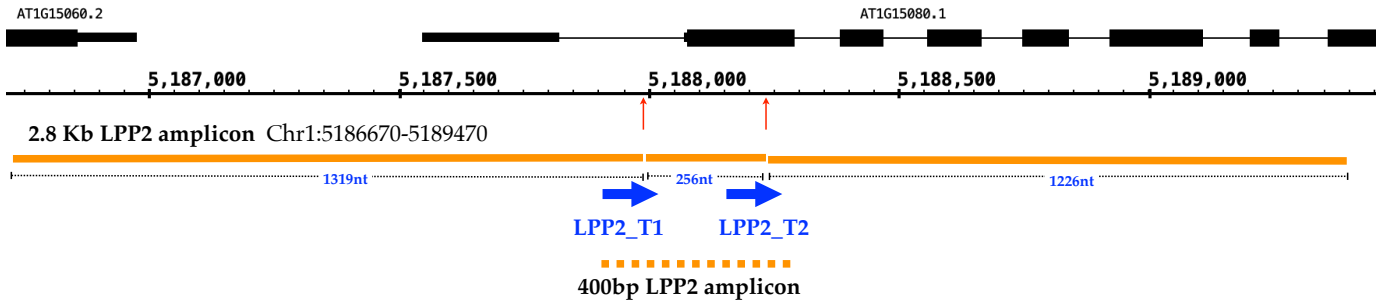
AT1G15060.2
AT1G15080.1
5,187,000
5,187,500
5,188,000
5,188,500
5,189,000
2.8 Kb LPP2 amplicon Chr1:5186670-5189470
1319nt
256nt
1226nt
LPP2_T1
LPP2_T2
400bp LPP2 amplicon

(b)

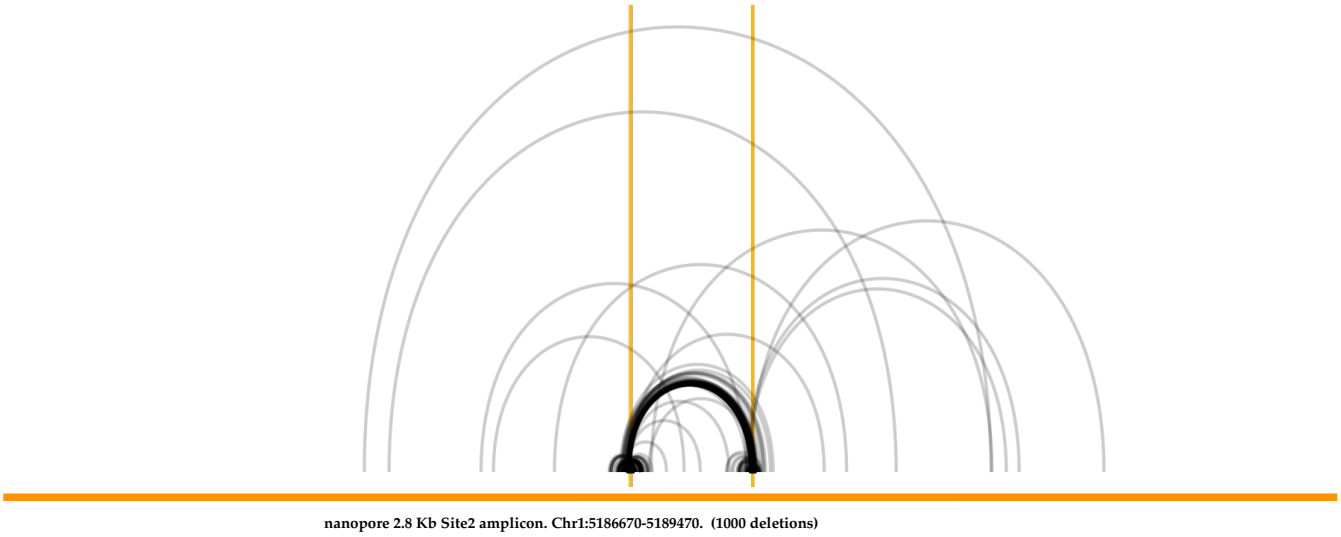
nanopore 2.8 Kb Site2 amplicon. Chr1:5186670-5189470. (1000 deletions)

(c)

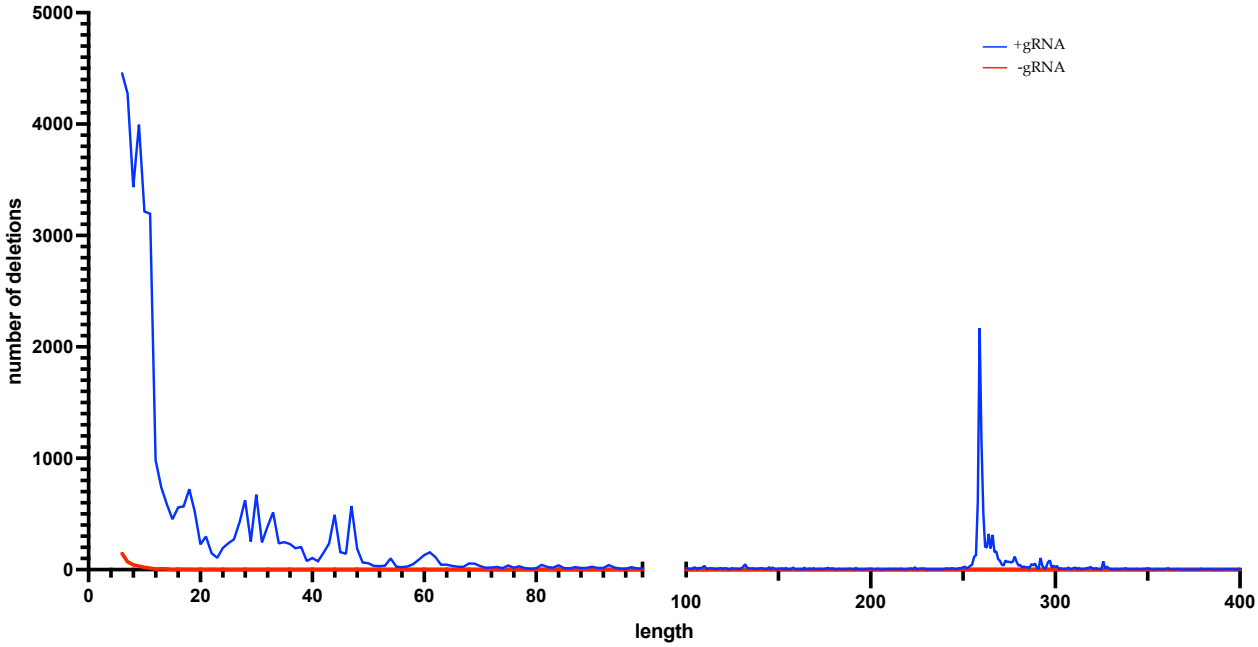
+gRNA
-gRNA
number of deletions
length
0
1000
2000
3000
4000
5000
0
20
40
60
80
100
200
300
400

Figure 5

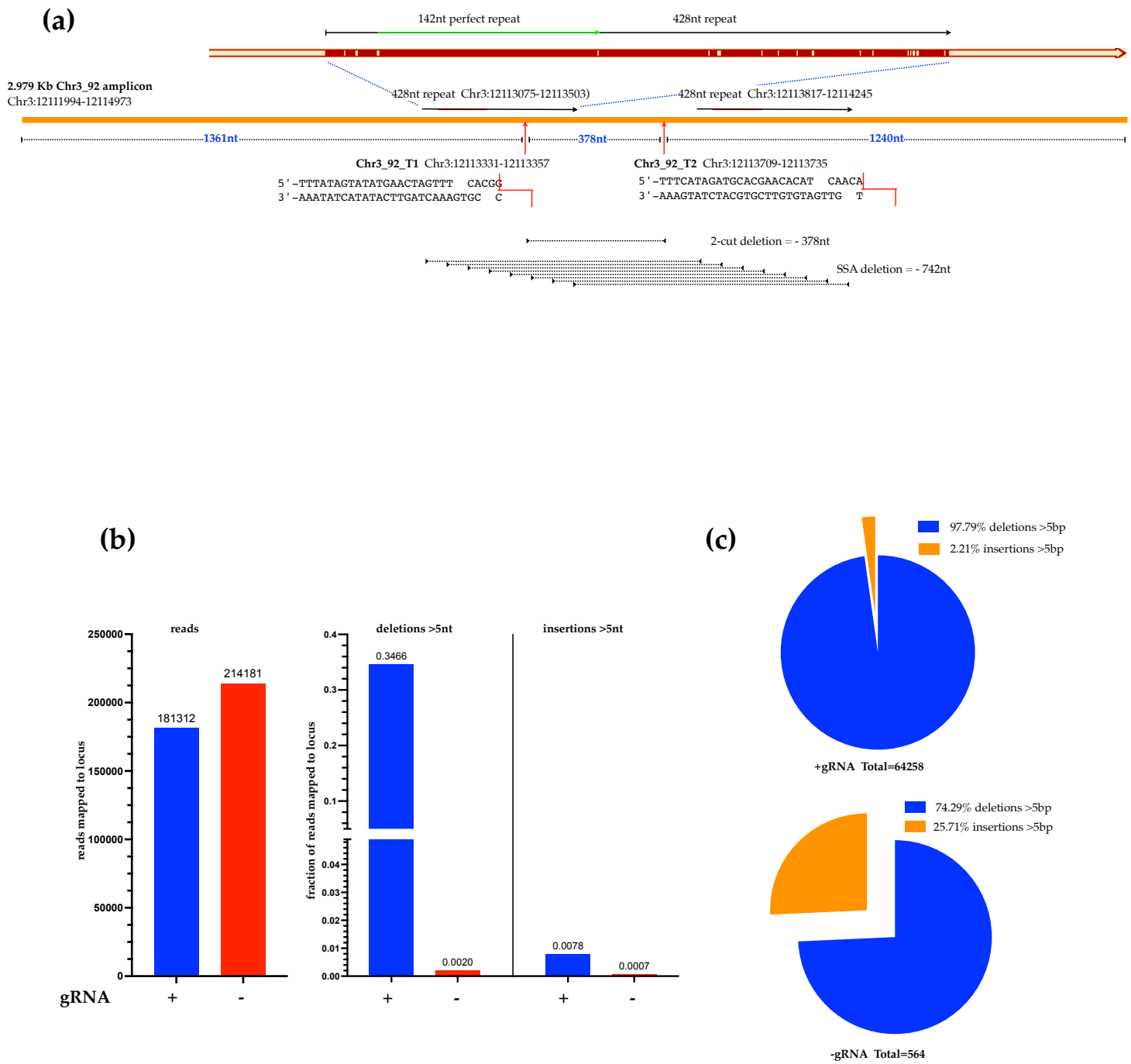
(a)
142nt perfect repeat
428nt repeat
2.979 Kb Chr3_92 amplicon
Chr3:12111994-12114973
428nt repeat Chr3:12113075-12113503)
428nt repeat Chr3:12113817-12114245
1361nt
378nt
1240nt
Chr3_92_T1 Chr3:12113331-12113357
5'-TTTATAGTATATGAACTAGTTT CACGG
3'-AAATATCATATACTTGATCAAAGTGC C
Chr3_92_T2 Chr3:12113709-12113735
5'-TTTCATAGATGCACGAACACAT CAACA
3'-AAAGTATCTACGTGCTTGTGTAGTTG T
2-cut deletion = - 378nt
SSA deletion = - 742nt
(b)
reads
deletions >5nt
insertions >5nt
reads mapped to locus
fraction of reads mapped to locus
181312
214181
0.3466
0.0020
0.0078
0.0007
gRNA
+
-
(c)
97.79% deletions >5bp
2.21% insertions >5bp
+gRNA Total=64258
74.29% deletions >5bp
25.71% insertions >5bp
-gRNA Total=564

Figure 6

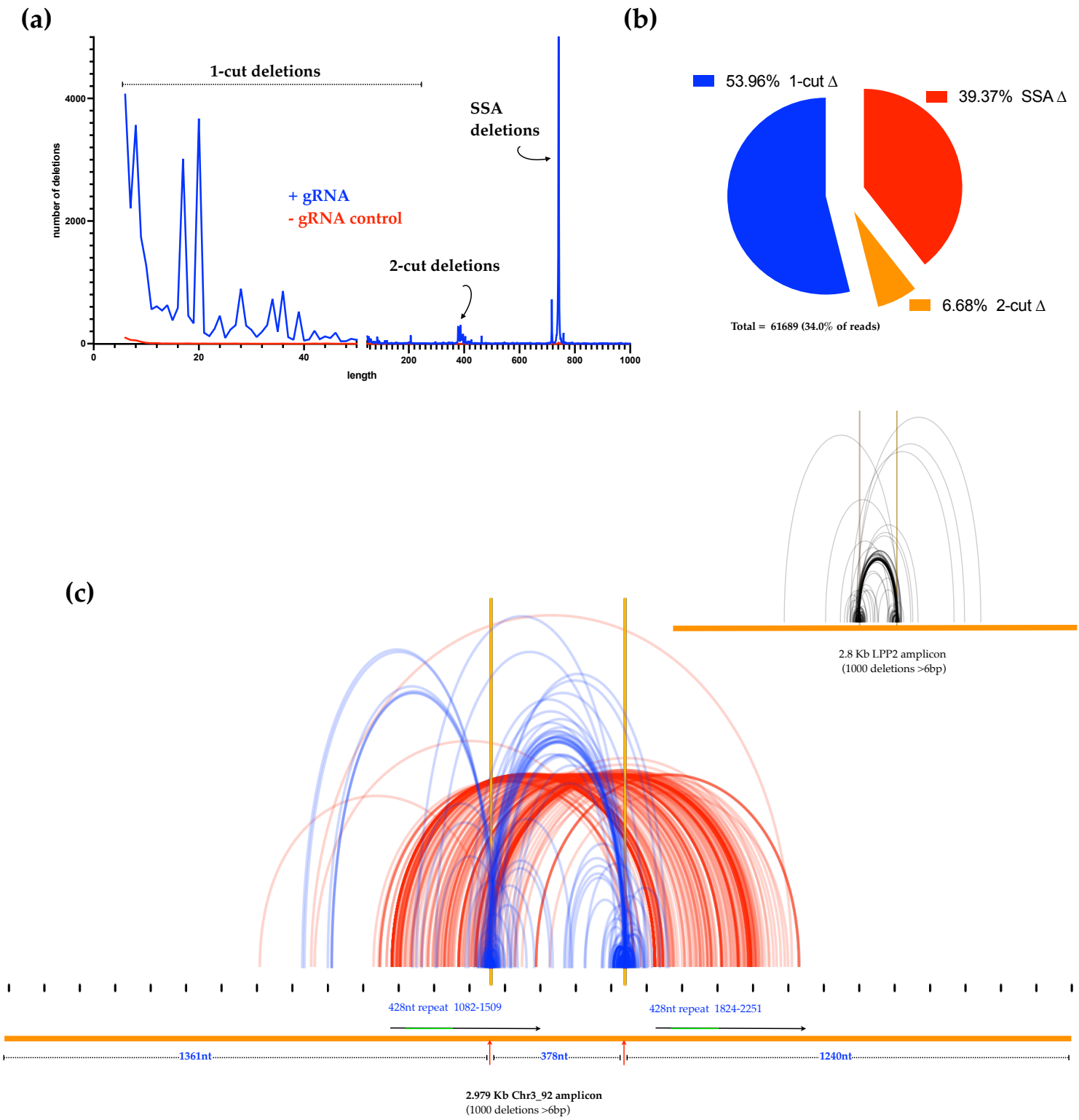
(a)
1-cut deletions
SSA deletions
+ gRNA
- gRNA control
2-cut deletions
number of deletions
length
(b)
53.96% 1-cut Δ
39.37% SSA Δ
6.68% 2-cut Δ
Total = 61689 (34.0% of reads)
(c)
2.8 Kb LPP2 amplicon
(1000 deletions >6bp)
428nt repeat 1082-1509
428nt repeat 1824-2251
1361nt
378nt
1240nt
2.979 Kb Chr3_92 amplicon
(1000 deletions >6bp)